Recent Advances in Atomic-Scale Spin-Polarized Scanning Tunneling Microscopy

ARTHUR R. SMITH[*], RONG YANG, AND HAIQIANG YANG[†].

Department of Physics and Astronomy, and Nanoscale and Quantum Phenomena Institute, Ohio University, Athens, OH 45701

ALEXEY DICK and JOERG NEUGEBAUER
Fritz-Haber-Institut der MPG, Faradayweg 4-6 D-14195 Berlin (Dahlem) Germany

WALTER R. L. LAMBRECHT
Department of Physics, Case Western Reserve University, Cleveland, OH 44106-7079

ABSTRACT   The Mn_3N_2 (010) surface has been studied using spin-polarized scanning tunneling microscopy at the atomic scale. The principle objective of the work is to elucidate the properties and potential of this technique to measure atomic-scale magnetic structures. The experimental approach involves the use of a combined molecular beam epitaxy/scanning tunneling microscopy system which allows the study of atomically clean magnetic surfaces. Several key findings have been obtained. First, both magnetic and non-magnetic atomic-scale information has been obtained in a single spin-polarized image. Magnetic modulation of the height profile having antiferromagnetic super-period of $c = 12.14$ Å (6 atomic rows) together with a non-magnetic superstructure having period of $c/2 = 6.07$ Å (3 atomic rows) was observed. Methods of separation of magnetic and non-magnetic profiles are presented. Second, bias voltage-dependent spin-polarized images show a reversal of the magnetic modulation at a particular voltage. This reversal is clearly due to a change in the sign of the magnetic term in the tunnel current. Since this term depends on both the tip's as well as the sample's magnetic local density of states, the reversal can be caused by either the sample or the tip. Third, the shape of the line profile was found to vary with the bias voltage, which is related to the energy-dependent spin contribution from the 2 chemically *in*equivalent Mn sites on the surface. Overall, the results shown here expand the application of the method of spin-polarized scanning tunneling microscopy to measure atomic-scale magnetic structures.

[*]Corresponding Author: Department of Physics and Astronomy,
Ohio University, Clippinger 251B, Athens, OH 45701, ph. (740) 597-2576, fax (740) 593-0433

[†] Present address: Department of Physics,
Texas A&M University, College Station, TX 77840, USA.

INTRODUCTION

Nanometer scale science and technology has been an area of intense research and development activity within the last 25 years. This is due to the fact that, although many other beginning points of this field may be suggested, only since the invention of the scanning tunneling microscope (STM) by Binnig, Rohrer and coworkers in 1981 has it been possible to directly observe objects of nanometer scale and smaller (down to single atoms) (Binnig, Rohrer, et al., 1982). This unique ability gives the STM great usefulness as a means of characterizing materials and devices of such ultra-small dimensions. As the ability to observe objects of this scale has developed, simultaneously have been great developments in many other fields, including the electronics and magnetics industries. While each of these industries is crucial to the world economy, amazingly the STM has been primarily used in its first 25 years to measure the *electronic* properties of surfaces. Only a tiny fraction of STM papers, and most of them within the last 5 years, have described the use of STM to measure the *magnetic* properties of surfaces (Bode et al., 2001; Bode et al., 2002, Heinze et al., 2000; Kleiber et al., 2000; Kubetzka et al., 2002, Kubetzka et al., 2003; Okuno et al., 2002; Vedmedenko et al., 2004; Wiesendanger et al., 1990; Wiesendanger et al., 1999; Yamada et al., 2003; Yang et al., 2002b). Many of these results have shown astonishing detail of the nanoscale magnetic structure of ferromagnetic (FM) and antiferromagnetic (aFM) surfaces.

In 2000, Heinze *et al.* reported the STM observation at low temperature of the ultimate spatial resolution of a magnetic structure, that being the magnetic structure of an aFM Mn monolayer on a W(110) substrate (Heinze et al., 2000). The magnetic period in this case was just 5.48 Å measured along the dense-packed [1-11] direction, which equals exactly 2 nearest-neighbor spacings. Since this surface can be viewed as row-wise aFM, the magnetic period of the rows (along the [1-10] direction) is 4.47 Å.

In 2002, Yang *et al.* reported the STM observation at room temperature of the magnetic structure of an aFM Mn_3N_2 (010) surface (Yang et al., 2002b). The top layer of atoms of the (010) face in fact has a similar row-wise magnetic structure to that imaged by Heinze *et al.*, but different in the structural details (to be discussed later). As measured along the [001] surface direction, the overall magnetic period measured is 12.14 Å, roughly 3 times larger than that of Heinze *et al.* However, Yang et al. did observe the shorter 6.07 Å period non-magnetic component.

In this paper, we review our recent work on the SP-STM imaging of Mn3N2 (010). We begin with an introduction to the surface using non-magnetic, atomically-sharp STM tips. Following that, the SP-STM imaging is presented of this surface, and methods of separation of magnetic and non-magnetic components are presented. Following this, we make a schematic comparison/contrast between our results and those of Heinze *et al.* in order to highlight the similarities and differences. We show in the next to last part of the paper bias-dependent SP-STM images in which the magnetic component is found to vary significantly with bias. The effective spin polarization is calculated, and some discussion is given to the role of the tip in this bias-dependence. Finally, some discussion is given to the subject of tip stability.

MATERIALS AND METHODS

The experiments described here are performed in a custom-designed ultra-high vacuum (UHV) system consisting of a molecular beam epitaxy (MBE) chamber coupled to a STM surface analysis chamber, which allows direct UHV transfer of samples from the growth chamber to the STM chamber. We have previously reported that η phase manganese nitride Mn_3N_2 (010) surface, a magnetic transition metal nitride surface, is ideal for the purpose of exploring atomic-scale SP-STM due to its row-wise aFM structure. The surface is prepared using a solid source effusion cell for Mn and an rf plasma source for N (Yang et al., 2001; Yang et al., 2002a). The substrate is MgO(001). Preparation of the substrate for growth is as follows: after being heated up to 1000 $^\circ$C for 30 minutes with the nitrogen plasma on, the MgO substrate temperature is lowered to 450 $^\circ$C prior to the growth of manganese nitride. The nitrogen flow rate is about 1.1 sccm (growth chamber pressure is 1.1×10^{-5} Torr) with the RF power set at 500 W. The Mn flux is about 3.5×10^{14}/cm^2 s.

The growth condition is monitored using reflection high energy electron diffraction (RHEED) which enables the determination of the surface crystal symmetry and surface lattice parameters. Following growth, the samples are investigated with *in-situ* STM and SP-STM. The bulk crystal structure of these samples has been verified using x-ray diffraction (XRD), and the bulk magnetic structure was verified by neutron scattering (NS), which showed that it agreed well with the crystal and magnetic structure previously determined for bulk Mn_3N_2 (Jacobs et al., 1984; Kreiner et al., 1992).

For growth under the stated conditions, the Mn_3N_2 film has the *c*-axis in the plane of the film (Yang et al., 2001; Yang et al., 2002a). Due to the 4-fold symmetry of the substrate, there are therefore 2 types of domains, A and B, which are equivalent by a rotation of 90º; additional domains due to twinning are also present; twins are at an angle of ~ 87.74º with respect to each other. All STM imaging is performed at 300 K in constant current (CC) mode.

Regarding the preparation of STM tips, for normal STM measurements we use W tips made by etching W wires in NaOH solution followed by dipping in clean H_2O. After loading into the UHV chamber, the tips are subsequently cleaned in UHV by electron bombardment. For SP-STM measurements, after the electron bombardment, we coat the cleaned W tips *in-situ* at 300 K with either: a) 5-10 ML of Mn; or b) 5-10 ML of Fe. The Fe-coated tips (T_C of Fe is 1043 K) are magnetized in the direction normal to the tip axis in a 40 mT field as described earlier (Yang et al., 2002b; Smith et al., 2004). Use of the Mn-coated tips has been found to be successful; justification for this was explained previously (Yang et al., 2002b) and briefly it is as follows: although the Néel temperature of Mn is only ~ 100 K (Martin et al., 1967), spin-polarized photoelectron diffraction of thin films of Mn have shown spin asymmetry up to ~ 500 K which was attributed to the surface atoms (Keen et al., 1998).

RESULTS AND DISCUSSION

A. Normal Atomic-Resolution Imaging of Mn_3N_2 (010) and Bias-Dependence

Shown in Fig. 1(a) is an STM image of the Mn_3N_2 (010) surface at small scale which was acquired using sample bias V_S = -0.4V and tunnel current It = 0.8 nA. The image of Fig. 1(a) was acquired with a tip of average sharpness (Yang et al., 2001). Clearly observable is the row-like structure of the surface; however, single atoms cannot be distinguished. Using a very sharp tip, as shown in Fig. 1(b), the row-like structure is also seen, and in addition, single atoms can be distinguished. This image was acquired with sample bias V_S = -0.3V and tunnel current It = 0.3 nA.

To understand the atomic resolution image in terms of a surface model, the image is compared with a bulk-like surface model, as shown in Fig. 1(c). This model is the bulk-like termination of the bulk model as first proposed by Jacobs and Kreiner (Jacobs et al., 1984; Kreiner et al., 1992). Although it is possible that the (010) surface could reconstruct, that is not found to be the case in experiment, and recent surface theoretical calculations also confirm that (Smith et al., 2004). There are two types of lattice sites for Mn atoms: sites having bonds with 2 surface N neighbors (Mn1 sites) and sites having bonds with 3 surface N neighbors and 1 backbonded N neighbor (Mn2 sites). The atoms which show in the atomic-resolution image as brighter clearly correspond with the Mn1 sites, whereas those which appear darker correspond to the Mn2 sites. Note that the Mn1 atoms lie in planes perpendicular to the surface which contain no N atoms, whereas the Mn2 atoms lie in planes perpendicular to the surface which contain N atoms. Thus the bulk can be considered as a repetition of 2 layers of MnN and 1 layer of Mn stacked along [001].

The detailed bias dependence of the atomic-resolution STM image of Mn_3N_2 (010) is displayed in Fig. 2. Four different biases are shown, a subset of those presented in the paper by Yang *et al.* (Yang et al., 2004). In all 4 images, Mn1 atoms are clearly observable. Mn2 atoms, however, are only clearly visible at larger magnitudes of bias voltage (+0.6V, -0.4V). At smaller magnitudes of bias voltage (+0.2V, -0.2V), the Mn2 atoms are less clearly resolved. A quantitative measure of this effect can be plotted, as shown in Fig. 2(b). Here, the ratio of the magnitude of the corrugation of Mn1:Mn2 is plotted vs. bias voltage; it is seen that this ratio is smaller at larger bias magnitudes. Another effect not so easily noticeable from the images of Fig. 2(a) is the overall corrugation magnitude variation with bias. This is plotted in Fig. 2(c), in which it can be seen that the magnitude is certainly larger at smaller bias magnitudes.

The bias-dependent Mn1:Mn2 corrugation ratio and overall corrugation vs. bias voltage were explained in our recent paper by Yang *et al.* in terms of the integrated local density of states (ILDOS) and simulated tip-sample spacing (Yang et al., 2004). Using values of the calculated LDOS integrated between the Fermi level (E_F) and E_F + eV_S in atom superposition simulations, the STM height data was simulated. Despite the fact that the calculated LDOS values were for bulk, good agreement was found with the STM height profiles vs. sample bias. The tip-sample distance d was also approximately determined from those simulations. It varied between 3.5 – 4.5 Å, with smallest value of d at V_S ~ -0.1 V and d = 4 Å at V_S = +0.2 V. At low bias voltages, to maintain constant tunnel current, the tip-sample distance is reduced; this results in the increased total corrugation at low bias magnitude. Increased resolution of Mn2 at larger bias magnitudes was explained in terms of a lowering of the ratio ILDOS(Mn1):ILDOS(Mn2) with increasing bias magnitude, such that the relative contribution from Mn2 is increased.

B. Spin-Polarized Imaging of Mn_3N_2 (010) at Atomic Scale

Using spin-polarized (magnetic) STM tips, images containing a periodic modulation of the apparent brightness of the rows of the Mn_3N_2 (010) surface, such as that shown in Fig. 3, can be obtained. The alternation of the brightness, actually the height of the rows, is due to the spin-polarized component of the tunnel current. This large image, showing two separate terraces, was acquired using a Mn-coated W tip at sample bias V_S = −0.2 V and tunnel current I_t = 0.3 nA. A step edge which is parallel to [100] is seen at the middle of the image. The arrows indicate the periodic alternation of the spin direction of the

antiferromagnetic structure. The row height modulation is continued across the step edge without any interruption. This should be the case since the row height modulation of the SP-STM image corresponds to the surface spin structure which in turn corresponds directly to the bulk spin structure.

Fig. 4(a) is another SP-STM image which was acquired using a Mn-coated W tip. This image spans slightly more than 3 magnetic periods of the surface structure obtained at a sample bias voltage $V_S =$ $-0.6V$ and tunnel current $I_t = 0.8$ nA. The period of the magnetic modulation is 2 rows, or $c = 12.14$ Å. The modulation is clearly seen in the average line profile displayed below in Fig. 4(b).

As explained by several authors (Heinze et al., 2000; Wortmann et al., 2001), the spin-polarized effect is due to the existence of a second term – the magnetic term - in the equation for the tunnel current. As with the non-magnetic term, this magnetic term is electronic in origin, being related to an imbalance in the spin-↑ LDOS and spin-↓ LDOS. The relevant quantities which determines the magnetic term are not the total magnetic moments of tip and sample ($\mathbf{\mu}_T$ and $\mathbf{\mu}_S$), but rather the spin-polarized LDOS of tip and sample near the Fermi level ($\mathbf{m}_T$ and $\mathbf{m}_S$).

When $\mathbf{m}_T$ and $\mathbf{m}_S$ are both finite and have the same sign, as projected along a common quantization axis, the tunnel current is increased; when they are finite and have the opposite sign, the tunnel current is decreased. It is interesting to note that the spin-polarized LDOS $\mathbf{m}$ near the Fermi level does not necessarily have the same sign as the magnetic moment $\mathbf{\mu}$. Thus it is possible that the tunnel current can be increased (decreased) even though the magnetic moments of tip and sample are anti-parallel (parallel).

The total tunnel current is related to the product of the non spin-polarized LDOS of tip and sample (n_T and n_S) and the vector dot product of $\mathbf{m}_T$ and $\mathbf{m}_S$. For either tip or sample, the non spin-polarized LDOS n is just the sum of up and down spin channels ($n_↑ + n_↓$) while the spin-polarized LDOS m is the difference of these two ($n_↑ - n_↓$). The height of the tip follows the formula:

$$z \sim \Delta I_t(\mathbf{R}_T, V, \theta) \sim \int n_T n_S(\mathbf{R}_T,V)\, d\varepsilon + \int m_T m_S(\mathbf{R}_T,V) \cos\theta\, d\varepsilon - \text{Constant} \qquad (1)$$

When m_T or m_S is zero (which implies $n_↑ = n_↓$), the spin-polarized term goes to zero and the line profile just corresponds to the non-magnetic component. Also, if the angle θ between $\mathbf{m}_T$ and $\mathbf{m}_S$ is 90º, the spin-polarized term goes to zero. But if these conditions are not true, then a spin-polarized component will exist.

Comparing the total CC line profile with the surface model shown in Fig. 1(c), one observes that the periodicity of the magnetic modulation corresponds to the periodicity of the Mn1 spin directions. The result indicates that there exists a component of the tip spin which is parallel (or antiparallel) to the surface spin directions.

In our earlier paper (Yang et al., 2002b), the angular dependence of the magnetic component was verified by measuring the row height modulation on either side of a surface domain boundary, such that the row directions on the two sides were at ~ 90º to each other; thus, the angle θ between the surface spin vector and the in-plane component of the tip spin vector was different by ~ 90º for the 2 sides, and the magnetic modulation was correspondingly different on the 2 sides of the domain boundary. A simple method was determined to use this angle-dependent data to determine the angle of the tip spin compared to the row direction. In this case, the angle was determined to be 27º, as depicted in Fig. 4(a).

C. Separation of Magnetic and Non-Magnetic Components

Since the total line profile as seen in Fig. 4(b) consists of magnetic and non-magnetic components, a method of separation was determined by Yang and Smith (Yang et al., 2002b). The method of separation is based on the consideration that the normal component has a period of $c/2$, whereas the magnetic component has a period of c. Therefore, if one takes a line profile $z(x + c/2)$ which is shifted by $c/2$ along the direction perpendicular to the rows and then subtracts it from the unshifted line profile $z(x)$, the normal components cancel out, leaving only the magnetic component. Similarly, if one adds these 2 line profiles together, the magnetic components cancel out, leaving only the normal component.

The separation procedure given below is derived in the following steps and referred to as Method A:

    1. assume Eq. (1) for the height of the tip above the magnetic surface

2. form the difference $\Delta z = z(x) - z(x + c/2)$

$$\Delta z \sim \int n_T[n_S(x) - n_S(x+c/2)] + \int m_T\{m_S(x)\cos[\theta(x)] - m_S(x+c/2)\cos[\theta(x+c/2)]\}$$

3. Since $n_S(x) = n_S(x+c/2)$, the non-magnetic part cancels out, and the remainder is of purely magnetic origin.
4. Next, if we assume reflection symmetry of the magnetic structure about Mn1, then $m_S(x) = m_S(x+c/2)$ and $\theta(x + c/2) = \theta + \pi - 2\beta$, where β = the (in-plane) angle of the tip moment with respect to the [100] row direction, then we get:

$$m_T m_S(x)\{\cos[\theta(x)] + \cos[\theta(x) - 2\beta]\} \sim z(x) - z(x+c/2)$$

5. Finally, in the case where the spins are not canted with respect to the [100] row direction, $\beta = \theta$. In this case, the following equation for the magnetic component is derived:

$$\int m_T m_S(x)\cos[\theta(x)] \sim [z(x) - z(x+c/2)]/2 \qquad \text{(magnetic component)} \qquad (2)$$

6. For the non-magnetic component, we follow a similar procedure but taking the sum $z(x) + z(x + c/2)$ to arrive at:

$$\int n_T n_S(x) \sim [z(x) + z(x+c/2)]/2 + C \qquad \text{(non-magnetic component)} \qquad (3)$$

The result of applying these 2 equations is that from the height profile data, the 2 separate components are obtained; these 2 components are the energy convolution integrals of the sample and tip LDOS and magnetic LDOS. If one assumes (or has additional knowledge) that the tip LDOS and magnetic LDOS are constants over the relevant energy window, then n_T and m_T can be taken outside the integral. However, in general this may not be true.

The spin-polarized line profile data of Fig. 4(b) is decomposed using equations (2) and (3) (method A), resulting in the separated line profiles shown in Fig. 4(c). The result shows that the normal component has the typical sinusoid-like line profile with period of $c/2$ obtained with non-magnetic STM tips. The non-magnetic peak-to-valley amplitude in this case is ~ 0.2 Å. The magnetic component (obtained with the same tip) clearly has period $= c$ and magnetic amplitude ~ 0.025 Å. Also, at this bias voltage, a trapezoidal shape is observed. In section (F), the origin of this shape will be discussed in more detail.

A more subtle effect which can be noticed from the magnetic line profile is a slight slanting of the trapezoidal shapes. While this effect may be related to inaccuracy in determining which points to subtract from each other and the fact that we are looking at the difference between 2 large quantities (the total height profile amplitude is much larger than the magnetic profile amplitude), variation of the method with one pixel shift of the points subtracted does not remove this effect. To explore if this effect could be related to some physical mechanism, a new subtraction procedure was developed which can allow the possibility of spin canting relative to the [100] direction – this is called method B. Method B is derived as follows:

1. Begin with the same expression (Eq. 1) as with method A for z

2. Form the difference $z(x) - z(c/2 - x)$:

$$\Delta z \sim \int n_T[n_S(x) - n_S(c/2 - x)] + \int m_T\{m_S(x)\cos[\theta(x)] - m_S(c/2 - x)\cos[\theta(c/2 - x)]\}$$

6

3. Assuming $n_S(x) = n_S(c/2 - x)$, the non-magnetic part cancels out, and the remainder is of purely magnetic origin. This can be done since the normal part of the surface LDOS must be symmetrical by mirror reflection about a Mn1 atom. However, this requires the non-magnetic aspect of our tip to be symmetrical. Because of this requirement, care must be exercised in the interpretation of the results of this method since tip asymmetries can exist.

4. The result is a magnetic quantity which does permit the possibility of spin canting.

$$\int m_T m_S(x)\cos[\theta(x)] \sim [z(x) - z(c/2 - x)]/2 \qquad \text{(magnetic component)} \qquad (4)$$

5. For the non-magnetic component, we follow a similar procedure but taking the sum $z(x) + z(c/2 - x)$ to arrive at:

$$\int n_T n_S(x) \sim [z(x) + z(c/2 - x)]/2 + C \qquad \text{(non-magnetic component)} \qquad (5)$$

Shown in Fig. 4(d) is the result of applying separation method B [Eqs. (4) and (5)] to the line profile data shown in Fig. 4(b). In practice, the method B is most easily applied by mirror-reflecting the $(n+1)^{st}$ peak about its midpoint and adding or subtracting this to the nth peak. One can see that the results are very similar to the case of method A; however, one notices that the slanting angle of the magnetic trapezoidal profile has changed such that the slope of the profile for the peak and valley have the same sign. It is possible to explain this asymmetrical profile using a spin canted model, as shown in Fig. 4(e). Given a tip spin at the angle shown, the profile is qualitatively obtained due to the cosine dependence of the magnetic term. Note that the angle of the tip spin is the same as the angle deduced experimentally for this data set from the domain boundary information (Yang et al., 2002b). However, proof for this explanation will require more data. Moreover, theoretical calculations taking into account spin canting are currently intractable, so it is not possible to confirm the explanation using theory. Finally, since a physical mechanism for this type of canting is not obvious, the effect will remain only as a possibility for the present time.

D. Comparison of Spin-Polarized Results with Those Obtained by Heinze et al. (Heinze et al., 2000)

Heinze et al. used Fe-coated and Gd-coated W tips to image the aFM structure of a Mn monolayer on W(110) (Heinze et al., 2000). Interestingly, they reported that although non-magnetic tips allowed to observe the atom-by-atom registry of the surface structure composed of chemically identical Mn atoms, use of the magnetic tips resulted in striped images in which the period of the stripes was equal to the magnetic period and the non-magnetic chemical contrast was absent. In our work, we found a different result in general, that with the use of magnetic-coated tips, we resolved the sum of the non-magnetic and magnetic components of the surface structure. It is thus useful to make a side-by-side comparison of these two independent results, as depicted in Fig. 5, which is a schematic illustration of the results on Mn_3N_2 (010) and Mn c(2×2)/W(110), and to try to understand the similarities and differences.

As can be seen in Fig. 5, the spatial arrangement of Mn atoms is very similar for the 2 different systems, Mn_3N_2 (010) and Mn/W(110). In either case, the surface Mn atoms form a centered rectangular lattice with their magnetic moments alternating in direction from row to row, with rows along [100] for Mn_3N_2 (010) and along [001] for Mn/W(110). Although the lattice constants and a:b ratios are slightly different (b = c/3 = 4.04 Å for Mn_3N_2 vs. b = 4.47 Å for Mn/W(110), for comparison in Fig. 5 we have normalized the 2 lattices along the x-direction.

If there were no other important differences between the 2 surfaces, then it would be very surprising to see the very different results obtained for the 2 cases - namely, for Mn/W(110), a purely magnetic component was found having period equal to 2 atomic rows and no normal component, whereas for Mn_3N_2 (010), a magnetic component was found with period 6 atomic rows and a normal component was also found with period 3 atomic rows. On the other hand, for Mn/W(110), with non-magnetic tips the

normal component with period equal to 1 atomic row was seen, and also for Mn_3N_2 (010), with non-magnetic tips the normal component with period equal to 1 atomic row was also seen, as shown here in Figs. 1 and 2.

It is thus important to consider the effect of the N atoms on Mn_3N_2 (010) which divide Mn into two categories, Mn1 and Mn2 [see Fig. 1(c)]. As deduced from neutron diffraction measurements, the bulk magnetic moments of Mn1 and Mn2 are 3.75 μ_B and (-)3.47 μ_B, respectively, or 3.38 μ_B and (-)3.65 μ_B, respectively, the two possibilities being indistinguishable from the powder diffraction patterns (Leineweber et al., 2000). Lambrecht et al. calculated the bulk magnetic structure of Mn_3N_2, finding bulk magnetic moments $\mu_{Mn1,bulk}$ = 3.0 μ_B and $\mu_{Mn2,bulk}$ = −2.8 μ_B. More recently, Dick and Neugebauer have calculated both the bulk and surface magnetic structure of Mn_3N_2. Their calculated bulk magnetic moments are $\mu_{Mn1,bulk}$ = 2.9 μ_B and $\mu_{Mn2,bulk}$ = −2.6 μ_B, which are comparable to the values calculated by Lambrecht. The calculated surface magnetic moments are slightly larger with $\mu_{Mn1,surface}$ = 3.4 μ_B and $\mu_{Mn2,surface}$ = −3.2 μ_B. The surface (and in fact bulk as well) magnetic moments are arranged as shown in the model of Fig. 5(a). From both experiment and theory, although the magnetic moments of Mn1 and Mn2 are similar, they are not equal. This is also true of the LDOS.

Plotted in Fig. 6(a) are the normal and magnetic bulk LDOS of Mn1 and Mn2 integrated from E_F to E_F + eV_S as functions of energy, as calculated by Lambrecht et al. using the full potential linear muffin-tin orbital (FP-LMTO) method (Lambrecht et al., 2003). Plotted in Fig. 6(b) are the same quantities, as calculated by Dick and Neugebauer employing density functional theory (DFT) in the spin-LDA approximation (Smith et al., 2004). One can see that these two bulk results [Figs. 6(a) and 6(b)] are very similar, showing excellent agreement of the two different calculations. In Fig. 6(c) are the same quantities for the surface, as calculated by Dick and Neugebauer. Importantly, for either surface or bulk, the spin-polarized LDOS in the vicinity of the Fermi level, m_{Mn1} and m_{Mn2}, are not generally equal and opposite, and neither are their integrals, (i.e. $\int m_{Mn1} d\varepsilon \neq -\int m_{Mn2} d\varepsilon$ for most energies), as one can clearly see from Fig. 6.

Therefore the magnetic period is really $3b = c$, which is $3\times$ the normalized magnetic period for Mn/W(110). We may refer to the surface magnetic structure as *triple*-row-wise aFM. So it is quite reasonable that the measured magnetic image for Mn_3N_2 (010) has period equal to c and not $c/3$. Similarly, since the LDOS for Mn1 and Mn2 are different, it is also quite reasonable that the non-magnetic component measured simultaneously with the same tip has a period equal to c/2, rather than c/6.

Still, we have shown that at the same sample bias voltages, a sharp tip is able to measure the smaller single atom-resolved non-magnetic image. The question therefore remains: is it possible using a sharper magnetic tip to measure the finer magnetic period of $c/3$? Heinze et al. gave an explanation for why they could not resolve the smaller spatial period non-magnetic image using their magnetic tips. By writing the change ΔI of the tunnel current I as a Fourier expansion in surface reciprocal lattice vectors, they showed that the terms involving the largest surface reciprocal lattice vectors (smallest spatial periods) are exponentially reduced in magnitude compared to terms involving smaller reciprocal lattice vectors (larger spatial periods). Thus, as a general principle, STM images will be dominated by corrugations having the largest spatial periods. In the results of Heinze et al. (Heinze et al., 2000), the magnetic component completely dominated the non-magnetic component to its total exclusion. In our results on Mn_3N_2 (010) (Yang et al., 2002b), similar reasoning could be applied to explain why our spin-polarized images have nonmagnetic spatial period of $c/2$ rather than $c/6$ and magnetic spatial period of c rather than $c/3$.

On the other hand, the fact that in our spin-polarized images of Mn_3N_2 (010) we can resolve a smaller spatial period of $c/2$ compared to the magnetic spatial period of c suggests that the magnetic component may contain (in fact, should contain) more information than a single Fourier component. This was first demonstrated in our earlier paper by Yang et al. (Yang et al. 2002b) in which the magnetic component was found to have a non-sinusoidal shape at $V_S = −0.6$ eV. In fact, a trapezoidal-like shape was found which will be further discussed in section F. The explanation for this profile shape is based on considering the contributions from both Mn1 and Mn2 atoms in adjacent atomic rows.

E. Bias-Dependence of Magnetic Line Profile Amplitude

Shown in Fig. 7 is a set of CC mode SP-STM images, each acquired from the exact same location on the sample surface. First of all, we see that magnetic modulation of the row structure is observed at all the displayed biases (V_S = -0.4, -0.2, +0.2, +0.6V). But, we see that for 3 out of the 4 images (-0.4, -0.2, and +0.2V), there are 2 high rows and 3 low rows, whereas at +0.6V there are 3 high rows and 2 low rows. Thus we find that between +0.2V and +0.6V, the magnetic modulation is reversed.

More information regarding these images is obtained by separating the magnetic and non-magnetic components using methods as described in Section C. The results (using Method A) are displayed in Fig. 8 where for each image, the total averaged line profile and also the separated components are displayed. First of all, it may be noticed that the amplitudes of the magnetic and non-magnetic components vary as a function of the bias. These amplitudes have been measured for an even larger set of bias voltages, and the results (peak-to-valley amplitudes) are plotted in Fig. 9(a). It is seen from Fig. 9(a) that the non-magnetic component is maximized at slightly positive sample bias, reaching a value of ~ 0.26 Å (peak-valley) at V_S = +0.1V. The general shape of the non-magnetic component amplitude curve is to be compared with the results plotted in Fig. 2(b) based on non-magnetic atomic-resolution data. The general agreement is fairly good, except that the maximum amplitude (peak-valley) for the sharper tip is ~ 0.49 Å at V_S = +0.2V.

The magnetic component, as seen in Fig. 8, varies in both magnitude and also in polarity, as indicated by the reversal seen between +0.2V and +0.6V in Fig. 7. The magnetic component amplitude (peak-valley), including sign, is also plotted in Fig. 9(a), including many other data points not presented in Fig. 7 or Fig. 8. The maximum magnetic amplitude (peak-valley) observed here is ~ 0.07 Å at V_S = −0.15V and goes to zero at V_S ~ +0.4V. Above 0.4V, the polarity is reversed.

F. Shape of Magnetic Line Profile

It is interesting to note the variation in the shape of the magnetic line profile with bias voltage. The trapezoidal shape seen at negative and small positive sample voltages (-0.6V to +0.2V) has already been mentioned in Section C. A more sinusoidal or even slightly triangular magnetic profile is observed at larger positive sample voltages. It is therefore clear that the shape of the line profile contains energy-dependent information.

Noting that the aFM half-period equals 3 single atomic rows – 1 row of Mn1 atoms and 2 rows (1 on each side of Mn1) of Mn2 atoms – Yang et al. gave an explanation for the trapezoidal shape of the magnetic profile at negative sample bias in terms of the magnetic ILDOS of Mn1 and Mn2 (Yang et al., 2002b). In particular, it was found using bulk spin-polarized LDOS calculations, that $\int m_{Mn2} d\varepsilon$ = 0.12 states/atom > $\int m_{Mn1} d\varepsilon$ = 0.02 states/atom at V_S = −0.7 eV. Using an atom superposition simulation and these ILDOS values, a flattened, trapezoidal-like profile was found. Therefore, comparing again with the work of Heinze et al. (Heinze et al., 2000) who observed a magnetic spatial period of just 2 atomic rows for Mn/W(110) (see Fig. 5) whereas our magnetic period is 6 atomic rows, the non-sinusoidal magnetic profile has particular significance. In Heinze's case, the Mn atoms in adjacent atomic rows were chemically equivalent (i.e. $\int m$(Mn atom in i[th] row) $d\varepsilon$ = $-\int m$[Mn atom in (i+1)[st] row] $d\varepsilon$. In our case [Mn$_3$N$_2$ (010)], Mn1 and Mn2 are in different bonding configurations (chemically *in*equivalent) and therefore do not have opposite ILDOS at all energies; thus, the observation of magnetic information having spatial period of only 2 atomic rows clearly depends on the energy window of integration (from E_F to E_F + eV_S). Although a 2 atomic-row magnetic modulation period is not obvious from the magnetic height profiles measured, in fact, since the trapezoidal line profile at negative bias is found to depend on magnetic contributions from individual Mn1 and Mn2 atomic rows, magnetic information from single atomic rows is actually observed.

More recently, the line profile results were re-examined using now-available surface theoretical calculations and SP-STM simulations performed by Alexey Dick and Joerg Neugebauer (Smith et al., 2004). In particular, the plot of surface ILDOS and surface magnetic ILDOS vs. energy, as seen in Fig. 6(c), was found to be very similar to that from bulk calculations as seen in Figs. 6(a) and 6(b), with some small, but consequential, differences.

Regarding similarity, $\int m_{Mn1} d\varepsilon$ and $\int m_{Mn2} d\varepsilon$ from the surface calculations are both positive for most of the range from 0V to –0.8eV, and at ~ –0.8 eV, $\int m_{Mn1} d\varepsilon \rightarrow 0$, similar to the bulk calculations. Thus, the atom superposition simulation of the magnetic component using surface magnetic ILDOS values agreed qualitatively with the results shown in our earlier paper (Yang et al., 2002b) which were based on the *bulk* theoretical calculations. Thus, both surface-based and bulk-based simulations confirm that the magnetic height profile of Mn_3N_2 (010) contains information from the individual Mn1 and Mn2 atomic rows.

Regarding the small differences between the results of surface and bulk calculations, the surface calculations found $\int n_{Mn2} d\varepsilon > \int n_{Mn1} d\varepsilon$ over the range 0 to –1 eV, whereas the bulk calculations had the opposite result, $\int n_{Mn1} d\varepsilon > \int n_{Mn2} d\varepsilon$ over the same energy range. This switch led to a 1.5 atomic row shift of the position of the normal component in the atom superposition simulation (Smith et al., 2004), placing the peak of the normal (non-magnetic) component midway between the Mn2 rows rather than centered on the Mn1 row. This of course does not agree with the experimental STM data, and it represents a breakdown of the atom superposition method.

It is interesting to note that at bias voltages in which $\int m_{Mn1} d\varepsilon$ and $\int m_{Mn2} d\varepsilon$ have the same sign, the spin arrangement can be viewed as ↑↑↑↓↓↓ rather than ↑↓↑↓↑↓, which is another way to understand why the magnetic line profile has a trapezoidal shape at those biases. It is important to note however, that the total magnetic moments still have aFM periodicity of ↑↓↑↓↑↓.

One of the key points of our recent work (Smith et al., 2004) is the direct, side-by-side comparison of the results of atom superposition with Tersoff-Hammann (T-H) simulations for SP-STM based on the energy-integrated surface LDOS. While some experimentally-observed trends in the height profile data have been reasonably well reproduced using atom superposition (see Yang et al., 2004), we have also found that atom superposition simulations can lead to inconsistencies with the non-magnetic STM data, as just discussed (Smith et al., 2004). Similarly, while atom superposition simulations reproduced reasonably well our experimental magnetic height profile data as we have shown previously (Yang et al., 2002b, Smith et al., 2004), we also found that the T-H simulations are in general necessary for correct simulation of spin-polarized STM data.

One of the main reasons for this is the fact that, for magnetic transition metal atoms, strongly directional spin-polarized orbital lobes can play a major role in the SP-STM image. In our recent paper (Smith et al., 2004), the spin-polarized orbital lobes are plotted in cross-section, and it is clearly seen that in the case of Mn1, although the sphere-summed magnetic ILDOS is net spin-↑, the orbital lobe the STM tip sees is spin-↓. The Mn2 atom, on the other hand, has a spin-↑ orbital lobe with the net sphere-summed magnetic ILDOS also spin-↑. Thus, the sphere-summed magnetic ILDOS may or may not have the same sign of the spin as the orbital lobe seen by the STM tip. However, after performing the T-H simulation using the surface orbital lobe magnetic ILDOS, we also found qualitative agreement with our experimental magnetic STM data at $V_S = –0.2V$ (Smith et al., 2004).

Due to the strongly localized nature of the spin-polarized orbital lobes, this T-H simulation contained sharp, atom-resolved magnetic features not found in our experiment to date. Improved agreement with the experimental magnetic height profile data was found by performing the T-H simulation using a 4-atom magnetic tip. This suggests that a sharper (i.e. triple-atom or single-atom) magnetic tip may be able to resolve sharper details of the surface magnetic structure. Obviously, production of such ultimate sharp, magnetic STM tips remains an experimental challenge.

G. Polarization Reversal of the Magnetic Profile

To obtain magnetic contrast reversal, the magnetic term in the tunnel current $\int \mathbf{m}_T \cdot \mathbf{m}_S \, d\varepsilon$ over the small energy range from the E_F to $E_F + eV_S$ must change sign with the voltage. This can occur in several ways. One way to obtain a reversal is for $\int \mathbf{m}_S \, d\varepsilon$ to change sign at a certain bias. Another way is for $\int \mathbf{m}_T \, d\varepsilon$ to change sign at a certain bias. Since very little is known about the magnetic state of the tip, it is generally very hard to determine which of these two factors is responsible.

Thinking of the tip-sample system as just a single entity, it is possible to calculate an effective spin polarization P_{EFF} of the tip-barrier-sample junction as a function of sample bias. P_{EFF} has been defined previously by Wiesendanger (Wiesendanger et al., 1990) as:

$$P_{EFF} = [I_{\uparrow\uparrow} - I_{\uparrow\downarrow}] / [I_{\uparrow\uparrow} + I_{\uparrow\downarrow}] \qquad (4)$$

Here, $I_{\uparrow\uparrow}$ denotes the tunnel current in which the spins of tip and sample are parallel, and $I_{\uparrow\downarrow}$ denotes the tunnel current in which the spins of tip and sample are anti-parallel. One of the first applications of this expression was by Wiesendanger et al., in the case of the Cr(001) topological aFM surface in which the spin alternates upon crossing a single monolayer-height step (Wiesendanger et al., 1990). In the case of a row-wise aFM surface, clearly $I_{\uparrow\uparrow}$ and $I_{\uparrow\downarrow}$ both occur periodically as a function of position on the surface. Since the STM is operated at constant current, the tip has to withdraw from or come closer to the surface depending on the magnetization directions of tip and sample. For Cr(001), this led to an alternation of the apparent step height. For a row-wise aFM surface, CC mode leads to the periodic modulation of the peak heights. In the case of CC mode, Wiesendanger et al. showed that Eq. (4) can be written as the following (Wiesendanger et al., 1990):

$$P_{EFF} = [\exp(A\sqrt{\Phi}\cdot\Delta s) - 1]/[\exp(A\sqrt{\Phi}\cdot\Delta s) + 1] \qquad (5)$$

Here, $A \approx 1.024$ eV$^{-1/2}$Å^{-1} and Φ is the local tunneling barrier height (for our surface we estimate $\Phi \sim 5$ eV). In the case of Cr(001), Δs was equal to the sum of the increase in tip position on one terrace compared to the normal tip position (0.1 Å) and the decrease in tip position on the next terrace (0.1 Å) which is then 0.2 Å. This was deduced by measuring the difference in measured height of consecutive steps (0.4 Å). In our case, Δs is similarly the sum of the increase in height of one peak (i.e. 0.02 Å) and the decrease in height of the next peak (i.e. 0.02 Å) for a total of 0.04 Å which is just the peak-to-valley amplitude of the magnetic modulation. The result for P_{EFF} for Mn_3N_2 (010) is shown in Fig. 9(b) (black line) which shows that the polarization is largest at $V_S \sim -0.1$ V. P_{EFF} decreases for more negative bias reaching a local minimum at $V_S \sim -0.71$V. P_{EFF} decreases for increasing positive sample bias, goes to zero at $V_S \sim +0.4$ V, then changes sign reaching a negative local maximum at $V_S \sim +0.67$V.

For comparison, also plotted in Fig. 9(b) is the ratio R of ½ the peak-to-valley magnetic amplitude to the non-magnetic peak-to-valley amplitude (red line). There is some similarity in the trend of R to P_{EFF}; however, the magnitude of R is larger than P_{EFF} by about a factor of 2 at various voltages.

The issue remains whether the observed magnetic contrast reversal occurring at $\sim +0.4$ V sample bias (corresponding to +0.4 eV in Fig. 6) can be simulated using only the sample's energy-dependent magnetic LDOS and a constant tip magnetic LDOS, or if instead it is due to a variable tip magnetic LDOS. As can be seen from Figs. 6(a), 6(b), or 6(c), $\int m_{Mn1}d\varepsilon$ is positive for all energies above the zero-crossing point (at ~ -0.8eV) except at the origin. On the other hand, $\int m_{Mn2}d\varepsilon$ changes sign from positive to negative as energy goes from negative to positive. Despite this sign change for Mn2, the competition between the effects of Mn1 and Mn2 on the magnetic profile make it not possible to explain the reversal by simple inspection of the magnetic ILDOS, and surface simulations are required. Moreover, full T-H simulations are required in general for reasons explained near the end of section F. Therefore, the theoretical explanation for the observed contrast reversal will be addressed in a future paper.

H. Spin-Polarized STM Tips

The magnetic LDOS of the STM tip is critical for the observation of spin-polarized images. Part of the difficulty of SP-STM is stabilizing the magnetic state of the tip. We have found that small changes to the tip during scanning are sufficient to modify the tip and change its magnetic behavior (Smith et al., 2004). Shown in Fig. 10 are two images of the same exact surface region of Mn_3N_2 (010), which were acquired by the same MnN-coated W tip but some time apart. As seen, the two images are completely different – one showing spin-polarization, one showing no spin-polarization. This result was obtained without

intentionally modifying the tip using voltage pulsing. It suggests that very small changes to the tip atom configuration are enough to affect the magnetic LDOS, such as picking up or dropping off one, or a few, tip atoms. Another point is that we have shown that aFM probe tips (i.e. Mn- or MnN-coated) can be used for atomic-scale SP-STM imaging of aFM surfaces. The use of aFM probe tips in SP-STM at nanometer scale was previously demonstrated by Kubetzka et al. on a FM surface [Fe/W(110)] (Kubetzka et al., 2002). A key advantage of an aFM probe tip is that it has a vanishing stray magnetic field and therefore should not disturb the sample spin structure being measured.

ACKNOWLEDGEMENTS

REFERENCES

Binnig G, Rohrer H, Gerber Ch, Weibel E.1982.Tunneling through a controllable vacuum gap. Appl. Phy. Lett. 40:188-180.

Bode M, Pietzsch O, Kubetzka A, Heinze S, Wiesendanger R. 2001. Experimental evidence for entra-atomic noncollinear magnetism at thin film probe tips. Phy. Rev. Lett. 86:2142-2145.

Bode M, Heinze S, Kubetzka A, Pietzsch O, Nie X, Bihlmayer G, Blügel S,Wiesendanger R. 2002. Magnetization-direction-dependent local electronic structure probed by scanning tunneling spectroscopy. Phy. Rev. Lett. 89:237205-8.

Heinze S, Bode M, Kubetzka A, Pietzsch O, Nie X, Blügel S, Wiesendanger R. 2000. Real-space imaging of two-dimensional antiferromagnetism on the atomic scale. Science 288:1805-1808.

Jacobs H, Stüve C. 1984. Hochdrucksynthese der η-phase im system Mn-N:Mn3N2. J Less-Common Met. 96:323−329.

Keen AM, Baker S H, Binns C, Mozley SN, Norris C, Derbyshire HS, 1998. Spin-polarized photoelectron diffraction of nanoscale manganese structures. Sol. Stat. Commu. 107:523- 526.

Kreiner G, Jacobs H. 1992. Magnetische Struktur von η-Mn_3N_2. J Alloys Compd 183:345−362.

Kleiber M, Bode M, Ravlić R, Wiesendanger R.2000. Topology-Induced Spin Frustrations at the Cr(001) Surface Studied by Spin-Polarized Scanning Tunneling Spectroscopy. Phy. Rev. Lett. 85:4606-4609.

Kubetzka A, Bode M, Pietzsch O, Wiesendanger R. 2002. Spin-Polarized Scanning Tunneling Microscopy with Antiferromagnetic Probe Tips. Phys. Rev. Lett. 88:057201-4.

Kubetzka A, Pietzsch O, Bode M, Wiesendanger R. 2003. Spin-Polarized Scanning Tunneling Microscopy Study of 360ºC walls in an exteral magnetic field. Phys. Rev. B. 88:R020401-4 .

Lambrecht WRL, Prikhodko M, Miao MS. 2003. Electronic structure and magnetic interactions in MnN and Mn3N2. Phy. Rev. B. 68:174411-174422.

Leineweber A, Niewa R, Jacobs H, Kockelmann W, 2000. The Manganese Nitrides η-Mn_3N_2 and θ-Mn_6N_{5+x}: Nuclear and Magnetic Structures. J. Mater. Chem. 10:2827-2834.

Martin D. 1967. Magnetism in solids, Ilife books LTD. London, P67.

Okuno SN, Kishiand T, Tanaka K. 2002. Spin-Polarized Tunneling Spectroscopy of Co(0001) Surface States. Phy. Rev. Lett. 88:066803-066806.

Smith AR, Yang R, Yang HQ, Lambrecht WRL, Dick A, Neugebauer J. 2004. Aspects of spin-polarized scanning tunneling microscopy at the atomic scale: experiment, theory, and simulation. Surf. Sci. 561:154-170.

Vedmedenko EY, Kubetzka A, Bergmann KV, Pietzsch O, Bode M, Kirschner J, Oepen HP, Wiesendanger R. 2004.Domain Wall Orientation in Magnetic Nanowires. Phys. Rev. Lett. 92:077207-10.

Wiesendanger R, Guntherodt H -J, Guntherodt GG, Gambino RJ, Ruf R. 1990. Observation of vacuum tunneling of spin-polarized electrons with the scanning tunneling microscope. Phys. Rev. Lett 65:247-250.

Wiesendanger R., Bode M, Getzlaff M, 1999. Vacuum-tunneling magnetoresistance: The role of spin-polarized surface states. Appl. Phys. Lett. 75:124-126.

Wortmann D, Heinze S, Kurz Ph, Bihlmayer G, Blügel S, 2001. Resolving complex atomic-scale spin structures by spin-polarized scanning tunneling mocroscope. Phys. Rev. Lett. 86:4132- 4135.

Yamada TK, Bischoff MMJ, Heijnen GMM, Mizoguchi T, Kempen HV, 2003. Observation of Spin-Polarized Surface States on Ultrathin bct Mn(001) Films by Spin-Polarized Scanning Tunneling Spectroscopy. Phys. Rev. Lett. 90:056803-056806.

Yang HQ, Al-Brithen H, Smith RA, 2001.Structural and magnetic properties of η-phase manganese nitride films grown by Molecular Beam Epitaxy. Appl. Phy. Lett. 78:3860-3862.

Yang HQ, Al-Brithen H, Smith RA, Trifan E, Ingram DC, 2002a. Crystalline phase and orientation control of manganese nitride films grown on MgO(001) by Molecular Beam Epitaxy. J. Appl. Phy.91:1053-1059.

Yang HQ, Smith R A, Prikhodko M, Lalter RL. 2002b. Atomic-scale spin-polarized scanning tunneling microscopy applied to Mn_3N_2 (010). Phy. Rev. Lett. 89:226101-226104.

Yang HQ, Yang R, Smith AR, Lambrecht WRL. 2004. Atomic-scale structure of η-phase Mn_3N_2 (010) studied by scanning tunneling microscopy and first-principles theory. Surf. Sci. 548:117-128.
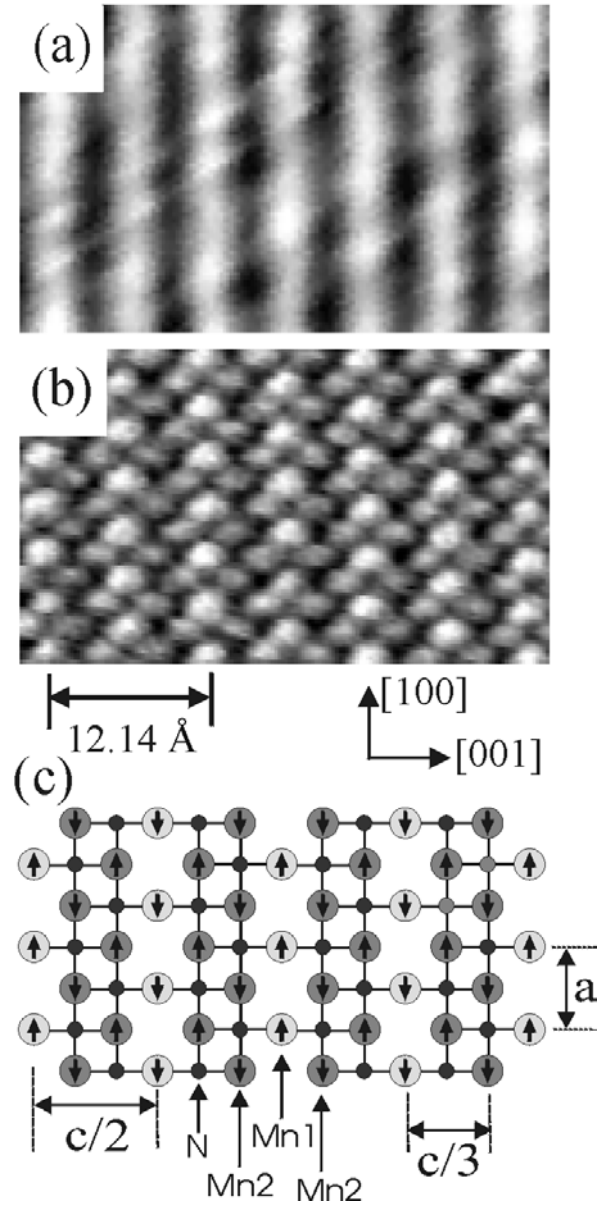
Fig. 1 (a) Normal STM image of η-Mn_3N_2 (010) surface acquired with non-magnetic tip at $V_S = -0.4$ V and $I_t = 0.8$ nA. (b) Atomic resolution normal STM image acquired at $V_S = -0.3$ V and $I_t = 0.3$ nA. (c) Bulk terminated (010) surface model.
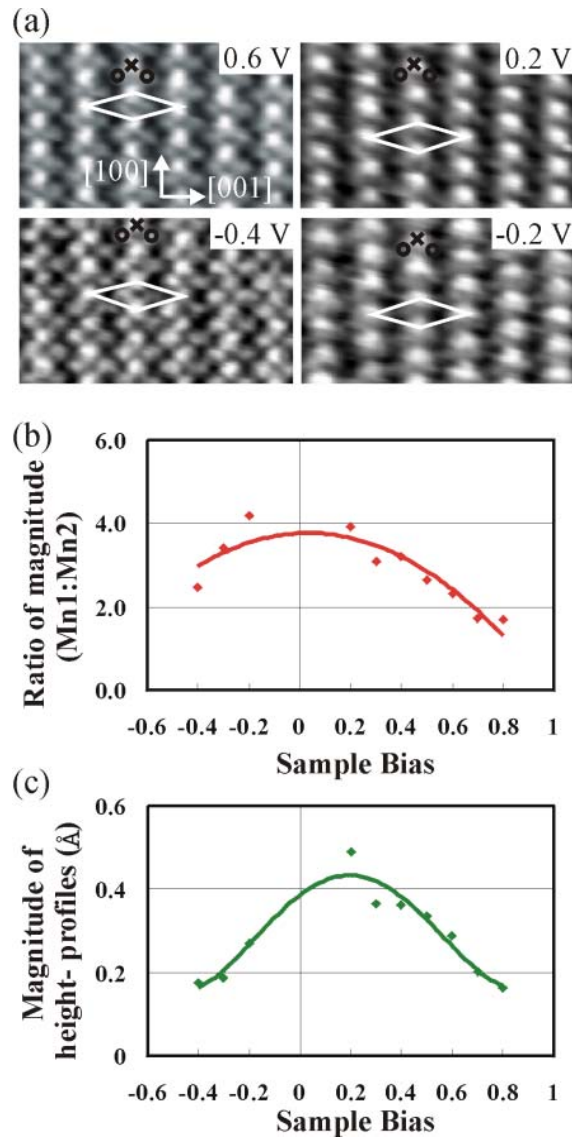
Fig. 2 (a) Bias-dependent normal atomic resolution STM images acquired with a tunnel current of 0.3 nA. Rhombus shows the non-magnetic unit cell of the surface. The × corresponds to the Mn1 atom, while the o corresponds to the Mn2 atom. (b) Ratio of the magnitude of the corrugation of Mn1 to that of Mn2 vs. sample bias. (c) The total height magnitude (peak-valley) as a function of sample bias. Solid curves are smoothed fits to the data points.
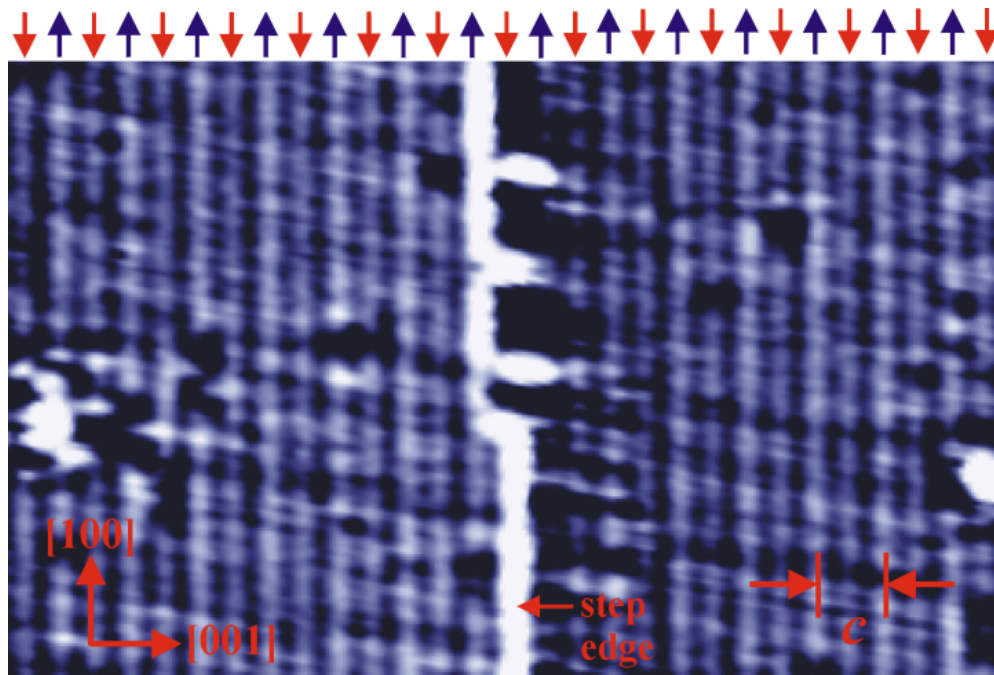
Fig.3. SP-STM image obtained using a Mn-coated W tip at a sample bias of $V_s = -0.2$ V and a tunnel current $I_t = 0.3$ nA.. The alternating spin structure is indicated by the arrows. The step edge appears bright due to the use of a local background subtraction to make contrast visible on both terraces.
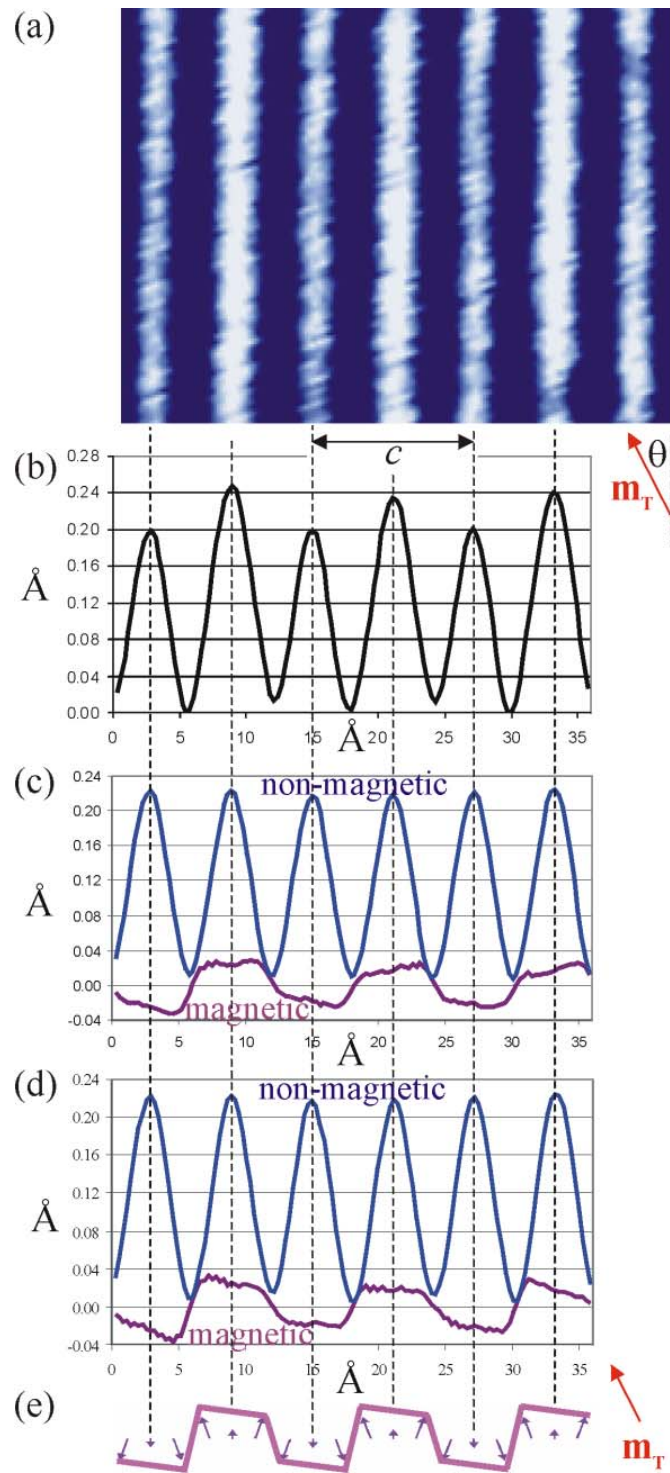
Fig. 4 (a) SP-STM image acquired using a Mn-coated W tip at $V_S = -0.6$ V and $I_t = 0.8$ nA. (b) Averaged line profile $z(x)$ corresponding to the SP-STM image in part (a); (c) separated components according to method A; (d) separated components according to Method B; (e) canted spin model. Color coding is non-magnetic (blue) and magnetic (purple).
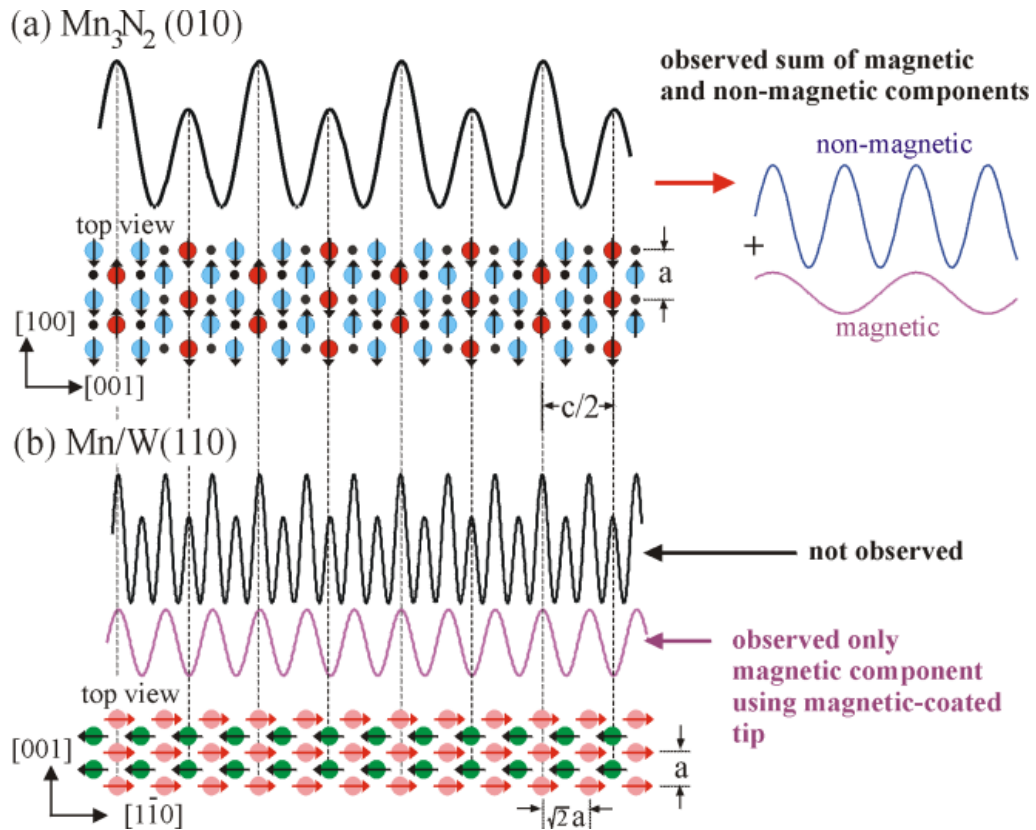
Fig. 5 Comparative diagram between SP-STM results on Mn_3N_2 (010) by Yang et al. and Mn/W(110) by Heinze et al. (a) schematic total line profile with top view surface model of Mn_3N_2 (010) and separated components; (b) schematic line profile obtained (only magnetic) with top view surface model of Mn/W(110); also shown is the fictitious total line profile including non-magnetic part which was not obtained. Surface models have been normalized to have the same x-direction atomic row spacing.
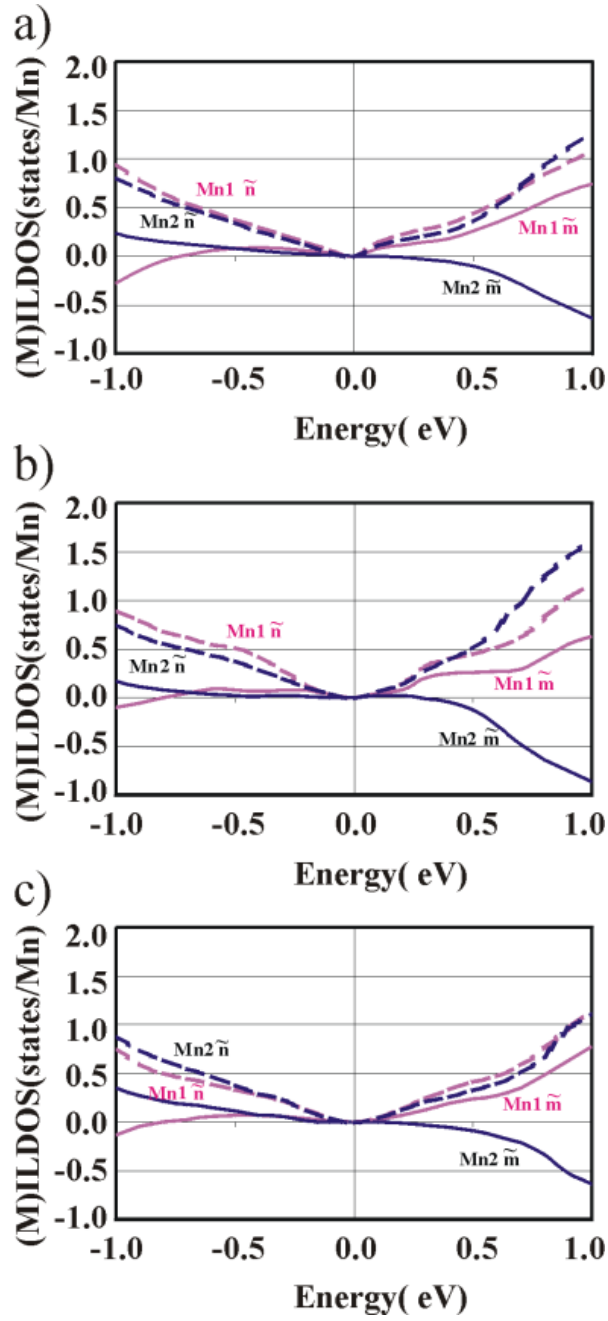
Fig. 6 (a) Normal and magnetic bulk ILDOS values ñ(Mn1), ñ(Mn2), and m̃(Mn1), m̃(Mn2) calculated by Lambrecht et al.; (b) Normal and magnetic bulk ILDOS values ñ(Mn1), ñ(Mn2), and m̃(Mn1), m̃(Mn2) calculated by Dick and Neugebauer; (c) Normal and magnetic surface ILDOS values ñ(Mn1), ñ(Mn2), and m̃(Mn1), m̃(Mn2) calculated by Dick and Neugebauer.

(a) +0.6 V

(b) +0.2 V

(c) -0.4 V

(d) -0.2 V

[100]

[001]

$c = 12.14$ Å
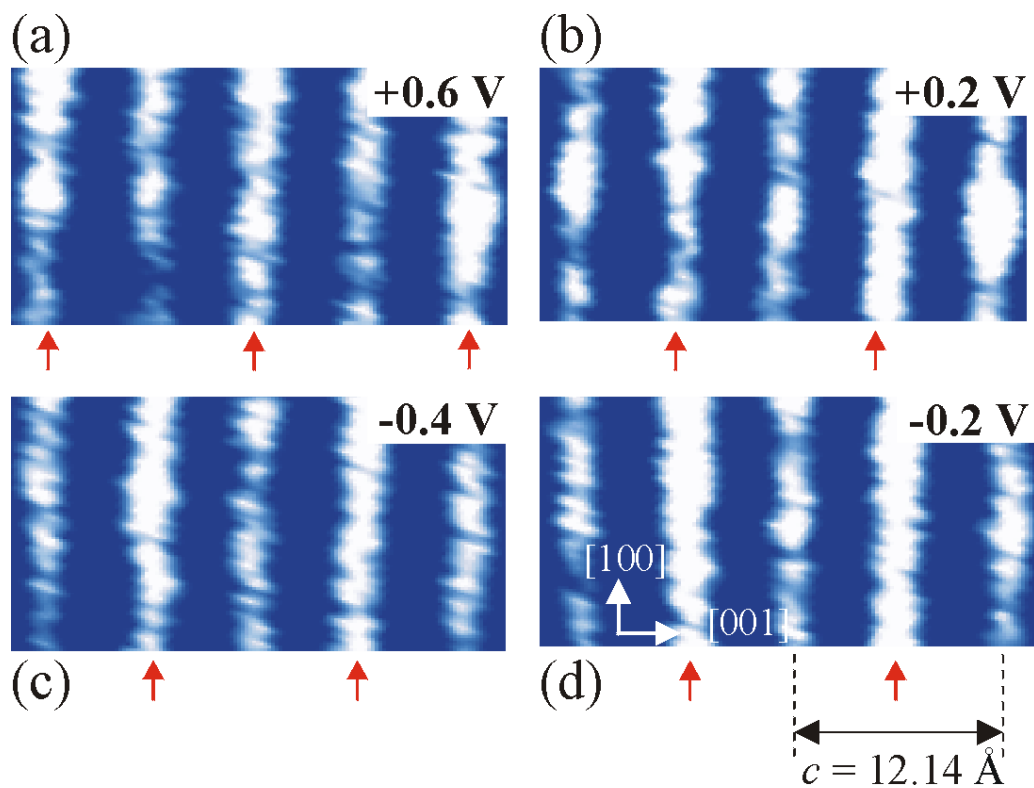
Fig. 7 A series of SP-STM images of Mn_3N_2 (010) acquired using a Fe-coated W tip taken at the exact same surface location. The sample bias is indicated in each part, and tunnel current $I_t = 0.3$ nA.
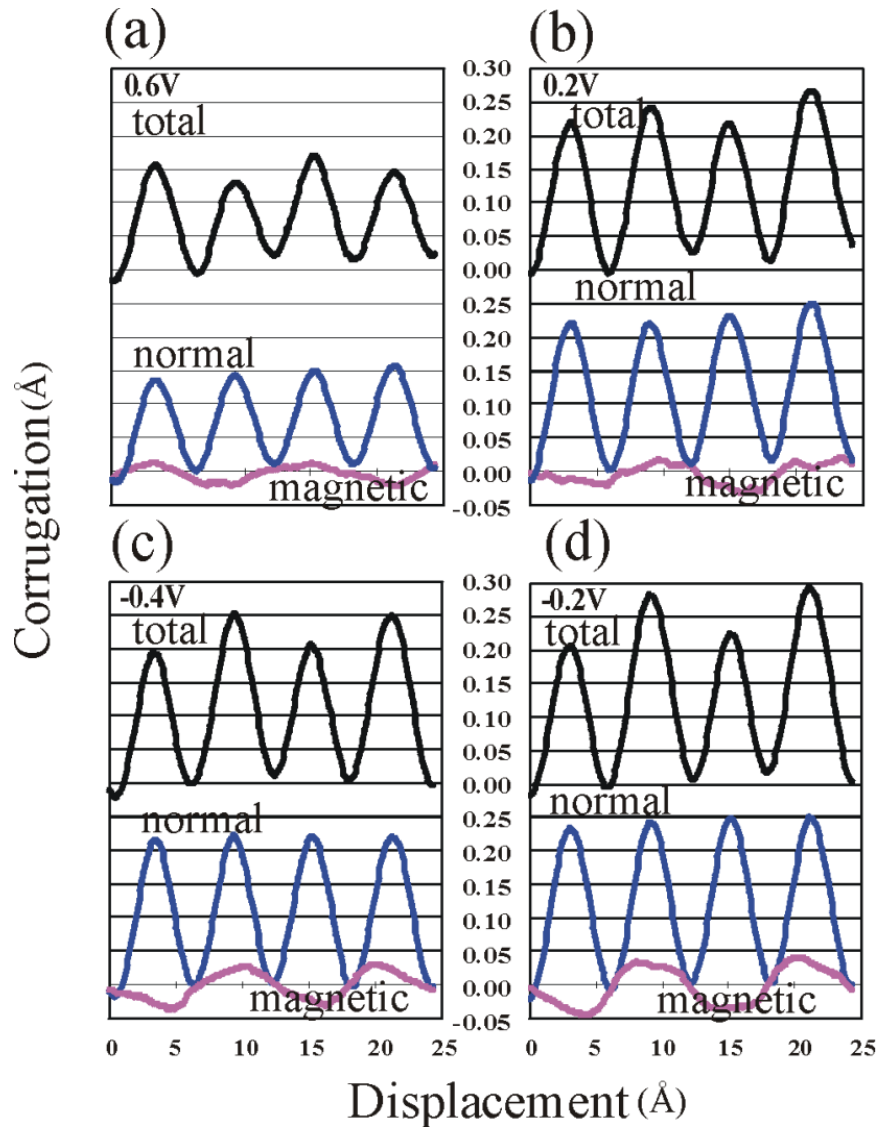
Fig. 8 Total height profiles corresponding to the SP-STM images of Fig. 7 and the separated non-magnetic (blue) and magnetic (purple) components. Sample bias is indicated in each part, and tunnel current I_t = 0.3 nA.
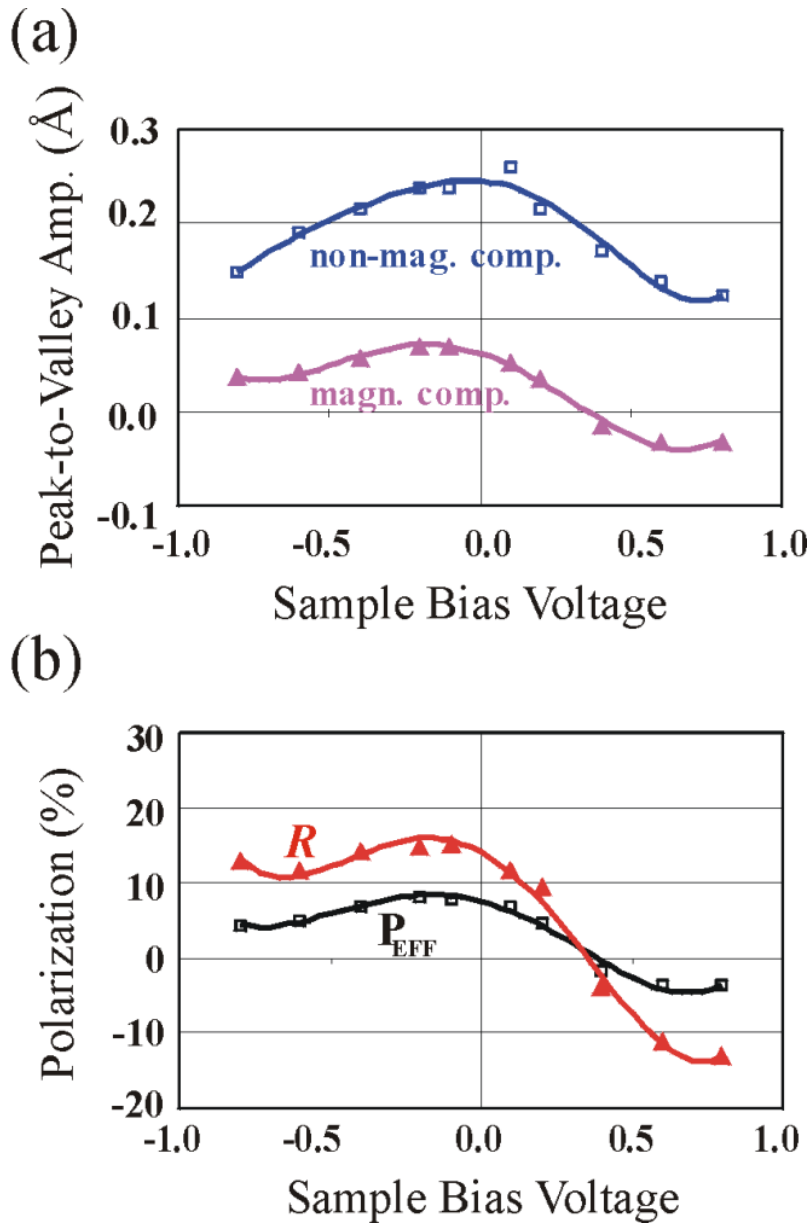
Fig. 9 (a) Peak-to-valley amplitudes of magnetic (purple) and non-magnetic (blue) components of the height profile as a function of sample bias. (b) The deduced junction polarization P_{EFF} from STM data using Eq. (5) (black) and the ratio R of ½ the magnetic peak-to-valley amplitude to non-magnetic peak-to-valley amplitude vs. sample bias from STM data (red).
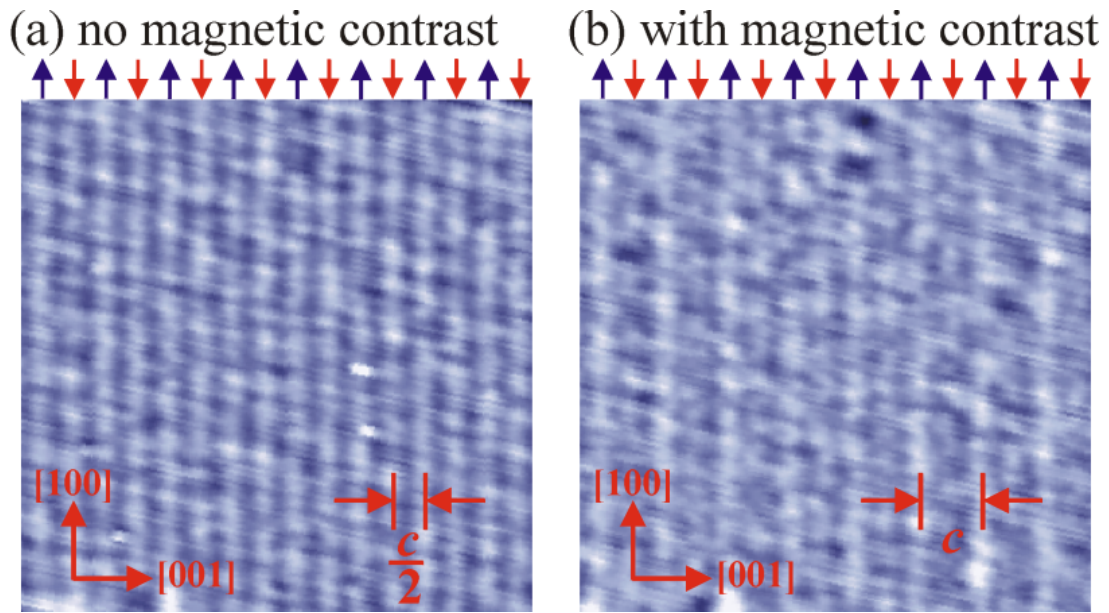
Fig. 10 STM images of the same surface area obtained using a MnN coated W tip but separated by some scanning time, showing (a) normal image, and (b) spin-polarized image. Both (a) and (b) were obtained at $V_s = -0.4$ V and $I_t = 0.5$ nA . The alternating spin structure is indicated by the arrows.